Analysis of Vibrational Resonance in Position Dependent Mass System Under an Amplitude Modulated Excitation

K. Suddalai Kannan,[1] M.V. Sethumeenakshi,[2] V. Chinnathambi,[1,*] and S. Rajasekar[3]

[1]*Department of Physics, Sadakathullah Appa College, Tirunelveli-627 011, Tamilnadu, India*

[2]*Department of Mathematics, Fatima College, Madurai-625 018, Tamilnadu, India*

[3]*School of Physics, Bharathidasan University, Tiruchirapalli 620 024, Tamilnadu, India*

Abstract

The phenomenon of vibrational resonance (VR) in a classical position-dependent mass (PDM) system under the influence of an amplitude modulated (AM) force with $\Omega >> \omega$ is numerically studied. The system provides an interesting scenario where PDM function makes a significant contribution to the occurrence of VR. With the results given by this paper one can weaken or enhance the weak low-frequency force in the PDM system by controlling the PDM parameters such as mass amplitude (m_0) and mass spatial nonlinearity (λ). The basic dynamical behaviours such as VR, period-doubling, reverse period-doubling, chaos, hysteresis and jump phenomenon have been investigated through bifurcation diagram, phase portrait and response amplitude.

PACS numbers: 05.45.-a,46.40.Ff, 05.90.+m

Keywords: Position dependent mass system, Amplitude modulated force, Vibrational resonance, Hysteresis, Chaos

*Electronic address: veerchinnathambi@gmail.com

1. Introduction

Recently, a phenomenon that is called vibrational resonance (VR) is investigated by numerical and analytical treatments. VR is commonly said to occur when a nonlinear system subjected to a biharmonic excitation consisting of a small amplitude resonant excitation and a large amplitude high-frequency excitation. Landa and McClintock [1] first reported the occurrence of VR in the weakly damped and overdamped bistable system numerically. Thereafter, an analytical investigation to confirm VR was carried out by Gitterman [2]. After these seminal works the features of this resonance have been analyzed in a variety of systems. For example, its occurrence has been analyzed in a monostable system [3], bistable system [4], a multistable system [5], an excitable system [6], a neuronal systems [7,8], a deformable potential system [9], a driven plasma [10], time delayed systems [11,12], and bistable gene transcriptional regulatory system [13]. Moreover, experimental evidences of VR have also been reported in a bistable optical cavity [14,15], an electronic circuit with a Chua's diode [6,16], a twin-well oscillator [17] and an array of hard limiters [18].

The study of position dependent mass (PDM) system is a subject of great interest in many branches of physics. In the PDM system the mass is dependent on a generalized coordinate either velocity or position or time or on a function of both position and time. In general, PDM systems are ubiquitous in nature and cut across different fields such as geometric optics [19], motion of rockets [20], variable mass oscillators [21], meteorites [22], aerology [22], inversion potential for NH_3 in density theory [23] and asteroids in the early solar systems [24]. In the past two decades numerous models have been used to illustrate the dynamics of PDM systems and much of the work was related to quantum variants [25]. Recently, classical PDM systems have also been considerable interest. In the classical picture, a position dependent mass function $m(x)$ gives rise to *forces quadratic* in the velocity which lead to nonlinear differential equations of motion in the Newtonian approach [26-29].

Generally in the VR studies, a nonlinear system driven by a weak periodic force, say, $f\sin\omega t$ is further subjected to a high-frequency force $g\sin\Omega t$ with $\Omega >> \omega$. Exploring the features of VR in systems with different types of setup of external force is a great significance. The goal of the present paper is to analyze VR by an amplitude modulated (AM) force can also be treated as consisting of a low-frequency force $f\sin\omega t$ and two high-frequency forces with frequencies $(\Omega+\omega)$ and $(\Omega-\omega)$. There are notable earlier studies on nonlinear systems subjected to AM force with $\Omega >> \omega$ [30-32].

The structure of this paper is as follows. To start with we introduce first the classical position-dependent mass model in Section-2. We consider the system with single-well potential in section 3. We describe the occurrence of VR and characterize it using the response amplitude Q. Hysteresis and a jump phenomenon is observed for sufficiently large values of the control parameters g, far after resonance. We find various dynamical behaviours such as bifurcations and chaos. Section 4 is devoted to the system with a double-well potential. We show the occurrence of enhanced VR, hysteresis and a jump phenomenon and various dynamical behaviours in the PDM system with double-well potential. Later, we explain the mechanism of resonance and dynamical behaviours of the system by using the response amplitude, bifurcation diagram and phase portrait. Finally, the conclusion of the research is given in section 5.

2. Classical Position-Dependent Mass Model

We consider classical systems for which the forces are only those derivable from a position-dependent potential so that Euler-Lagrange's equations of motion are of the form

$$\frac{d}{dt}\left(\frac{\partial L}{\partial \dot{x}}\right) - \left(\frac{\partial L}{\partial x}\right) = \Phi \tag{1}$$

where L is the Lagrangian function is also called Lagrangian quantity that characterizes the state of a physical system and Φ accounts for all the external contributions to the motion of the system from dissipative and driving forces, assume here to be $\Phi = -d\dot{x} + (f + 2g\cos\Omega t)\sin\omega t$. Where d is the damping coefficient and the amplitudes and frequencies of the AM force are f and ω for the low-frequency component and g and Ω for the high-frequency component, respectively. In classical mechanics, the dynamics of the PDM systems may be described by the Lagrangian function as

$$L(x, \dot{x}, t) = T - V(x) = \frac{1}{2}m(x)\dot{x}^2 - V(x) \tag{2}$$

Where $T = \frac{1}{2}m(x)\dot{x}^2$ is the kinetic energy of the system, $V(x)$ is the system's potential and $m(x)$ is the position-dependent mass function with x being position at time t. Using the Lagrangian function (Eq.2) in the Euler-Lagrangian equations, the corresponding Newton's equation of motion is given by

$$m(x)\ddot{x} + \frac{1}{2}m'(x)\dot{x}^2 + \frac{dV(x)}{dx} = \Phi \tag{3}$$

The prime in Eq.3 implies differentiation with respect to space variable x and the over dot indicates differentiation with respect to time. Apart from the various mass function, in this

paper, we adopt the simplest regular mass function without singularities

$$m(x) = \frac{m_0}{1 + \lambda x^2}, \tag{4}$$

where m_0 is a constant mass, equivalent to the mass amplitude and λ is the strength of the spatial nonlinearity in mass. The mass function $m(x)$ is bounded and defined over the entire real line $D(m_1) = \Re$ with its maximum,m_0, at $x = 0$ and vanishing at $\mid x \mid \rightarrow \infty$. The variation of mass with position is given by $m'(x) = -2\ m^2(x)\ x\ \gamma\ \lambda$, where $\gamma = \frac{1}{m_0}$. This mass function originally introduced by Mathews and Venkatesan [26] in relation to relativistic fields of elementary particles. The mass function (Eq.4) appears frequently in the modelling of diverse nonlinear mechanical systems [33,34,35]. In our present work, we assume a Duffing type oscillator potential, ie,

$$V(x) = \frac{1}{2}\ m(x)\ \omega_0^2\ x^2 + \frac{1}{4}\ \beta\ x^4\ , \tag{5}$$

where ω_0 is the oscillator's natural frequency and β is the stiffness constant which plays the role of the nonlinear parameter.

Substituting the values of $\Phi, m(x), m'(x)$ and $V(x)$ in Eq.(3), we get the equation of motion of the PDM-Duffing oscillator, ie.,

$$m(x)\ \ddot{x} - m^2(x)x\gamma\lambda\dot{x}^2 + d\dot{x} + m^2(x)\ \omega_0^2\ x + \beta x^3 = (f + 2g\cos\Omega t)\sin\omega t,\ \ \Omega >> \omega. \tag{6}$$

With the use of the formula $2\cos\Omega t\sin\omega t = \sin(\Omega + \omega)t + \sin(\Omega - \omega)t$, Eq.(6) takes the form,

$$m(x)\ \ddot{x} - m^2(x)x\gamma\lambda\dot{x}^2 + d\dot{x} + m^2(x)\ \omega_0^2\ x + \beta x^3 = f\sin\omega t + g\sin(\Omega+\omega)t + g\sin(\Omega-\omega)t,\ \ \Omega >> \omega. \tag{7}$$

When $\lambda = 0$ and unit mass $m(x) = 1$, Eq.(7) reduces to the well known Duffing oscillator equation driven by an AM force. The physical system (Eq.6) describes a dual frequency driven gas bubble in which the mass of the bubble is dependent on the bubble's radius, which is a spatial coordinate. By suitable mathematical manipulations in the Eq.(7) as given in the ref.[35], the following equation can be used to numerically analyze the various dynamical behaviours of the PDM-Duffing oscillator system

$$\begin{aligned} &\ddot{x} - \lambda(x - \lambda x^3 + \lambda^2\ x^5)\dot{x}^2 + d\gamma(1 + \lambda x^2)\dot{x} + \omega_0^2\ x + \delta x^3 + \xi x^5 = \\ &\gamma(1 + \lambda x^2)\ (f\sin\omega t + g\sin(\Omega + \omega)t + g\sin(\Omega - \omega)t),\ \ \Omega >> \omega. \end{aligned} \tag{8}$$

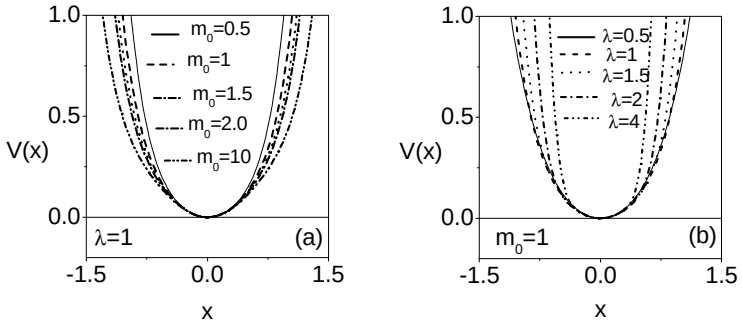

FIG. 1: (a) The system potential (Eq.9) for $d = 0.2, \beta = 1, \omega_0^2 = 1, \lambda = 1$ and $m_0 = 0.5, 1.0, 1.5, 2.0, 10.0$ (b) The system potential (Eq.9) for $d = 0.2, \beta = 1, \omega_0^2 = 1, m_0 = 1$ and $\lambda = 0.5, 1.0, 1.5, 2.0, 4.0$.

where $\delta = \beta\gamma - \lambda\omega_0^2$ and $\xi = \beta\gamma\lambda + \lambda^2\omega_0^2$. Eq.(8) is also known as the PDM-Duffing oscillator equation. The corresponding potential of the system is

$$V(x) = \frac{\omega_0^2}{2}\, x^2 + \frac{\delta}{4}\, x^4 \ + \frac{\xi}{6}\, x^6 \ . \tag{9}$$

The shape of the potential $V(x)$ depends on the parameters ω_0^2, γ and λ. It can be a single-well, double-well, single-well with double-hump, double-well with double hump and inverted single-well potentials. Recently, Roy-Layinde et al [35] examined and analyzed the VR phenomenon in double-well PDM-Duffing oscillator system driven by biharmonic force. In the present work, we numerically analyze the occurrence of VR in single-well and double-well PDM-Duffing oscillator system with AM force.

3. VR in the Single-Well PDM-Duffing Oscillator

In this section, we analyze the occurrence of VR in the system (Eq.8) with symmetrical single-well form of the potential $V(x)$. Consider the parametric choices of the single-well potential are $\omega_0^2 > 0$ and $\beta > 0$. The system potential (Eq.9) shown in Figs.1(a) and 1(b) for different values of the PDM parameters such as mass amplitude $m_0 (= 0.5, 1.0, 1.5, 2, 10)$ with $\lambda = 1$ and the strength of the spatial nonlinearity $\lambda (= 0.5, 1.0, 1.5, 2, 4)$ with $m_0 = 1$. In Fig.1(a), for a fixed value of λ, the width of the single-well potential increases as m_0 increases but in Fig.1(b) the width of the potential decreases as λ increases for a fixed value of m_0.

To numerically integrate the PDM-Duffing oscillator system (Eq.8) driven by an AM force, it is convenient to express it as a set of two coupled autonomous one dimensional

differential equations (ODEs) of the from

$$\dot{x} = y, \tag{10a}$$

$$\dot{y} = \lambda\left(x - \lambda x^3 + \lambda^2 x^5\right)\dot{x}^2 - d\gamma\left(1 + \lambda x^2\right)\dot{x} - \omega_0^2 x - \delta x^3 - \xi x^5 + \gamma\left(1 + \lambda x^2\right)\left((f + 2g\cos\Omega t)\sin\omega t\right) \tag{10b}$$

In Eq.(10) d, ω_0^2 and β are all system parameters. When $\Omega \gg \omega$, the amplitude modulated force can also be treated as consisting of a low-frequency force $f\sin\omega t$ and two high-frequency forces with frequencies $\Omega + \omega$ and $\Omega - \omega$.

In order to quantify the VR effect, we calculate the response amplitude Q of the system at the low-frequency ω. It is defined as ref.[1] $Q = \sqrt{Q_s^2 + Q_c^2}/f$ with

$$Q_s = \frac{2}{nT}\int_0^{nT} x(t)\sin(\omega t)dt \tag{11a}$$

$$Q_c = \frac{2}{nT}\int_0^{nT} x(t)\cos(\omega t)dt \tag{11b}$$

with $T = 2\pi/\omega$ is the period of the response and n is a positive integer. The $x(t)$ obtained by numerically solving the differential equation (Eq.8) using fourth-order Runge-Kutta algorithm with time step size $\Delta t = (2\pi/\omega)/200$. Numerical solutions corresponding to 500 drive cycles are left as transients. In all the calculations the initial conditions are chosen as $x(0) = 0.5$ and $\dot{x} = 0.5$ and the system and signal parameters are $\omega_0^2 = 1, \beta = 1, d = 0.2$ and $f = 0.05$.

We begin our examination of the phenomenon of VR in the system by first considering the case of constant mass (m_0). That is, the PDM-Duffing oscillator (Eq.10) in which $m(x) = m_0$ and $\lambda = 0$ corresponding to a Duffing oscillator with constant mass m_0. Figures 2(a-c) show the response amplitude curves depicting the dependence of response amplitude Q on the amplitude g of the high-frequency force for three values of mass amplitude $m(= 0.5, 1.0, 1.5)$ respectively. The other parameter values are $\lambda = 0, \omega = 1.5, \Omega = 15$ and $f = 0.05$. Here we see that the VR effect can be induced in the system even in the absence of mass spatial nonlinearity ($\lambda = 0$) with increasing mass amplitude m_0. The low-density peaks in Figs.2(a) and 2(b) appear at $0 < g < 352.23$ and $0 < g < 1095.52$ for $m_0 = 0.5$ and 1.0, respectively. Dense peaks appear beyond this regime. In Fig.2(c), almost low-density peaks appear throughout the entire regime. The system's response becomes significantly altered at higher values of Ω as shown in Fig.2(d). Figure 2(d) shows the dependence of

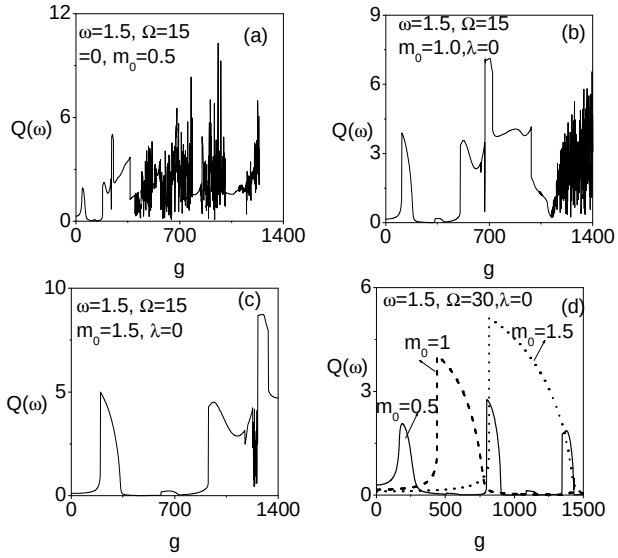

FIG. 2: The variation of response amplitude Q with g for three values of $m_0 = 0.5, 1.0, 1.5$ with (a-c) $Q = 15$, (d) $Q = 30$. Other parameters are set as $\omega_0^2 = 1, \beta = 1, d = 0.2$ and $\lambda = 0$.

response amplitude Q on the amplitude g of the high-frequency force for three values of $m_0 = 0.5, 1, 1.5$ with $\Omega = 30$. In Fig.2(d) we can clearly see the resonance at three values of g for $m_0 = 0.5$. The value of Q at $g_{VR} = 805.12$ is slightly higher than the values of other g_{VR}. For $m_0 = 1.0$ and 1.5, single resonance is observed at $g_{VR} = 500.15$ and 807.52 with an enhanced response amplitude Q which is clearly shown in Fig.2(d). The value of Q increases when m_0 increases.

In Fig.2(a), for $\Omega = 15$ a nonsmooth variation of $Q(\omega)$ is clearly seen for a certain range of values of g. To find the reason for this fact that, we consider the bifurcation diagram Fig.3 where the values of x are as $t = n(2\pi/\omega),\ n = 1, 2, ...$, after leaving sufficient transient motion. In the interval of $g \in [0, 175]$, where x is periodic with period $T = 2\pi/\omega$, the response amplitude varies smoothly. For $g \in [175, 1400]$ either higher periodic or chaotic motion occurs and Q is found to irregularly. However, the value of Q is nonnegligible. In Fig.2(d), for $\Omega = 30$, a smooth variation of $Q(\omega)$ is clearly seen in the entire range of values of g and x is periodic with period $T = 2\pi/\omega$, which is clearly seen in Fig.3(b).

Now, we analyzing the dependence of Q on m_0, ω and Ω when activating the mass spatial nonlinearity (λ) for the following cases.

(i) m_0 varied and λ fixed; (ii) m_0 fixed and λ varied

(iii) m_0, λ, Ω fixed and ω varied and (iv) m_0, λ, ω fixed and Ω varied.

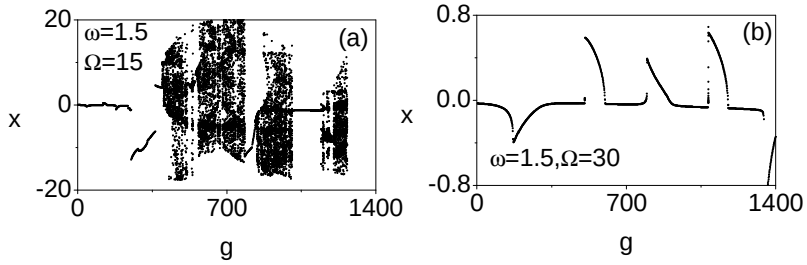

FIG. 3: (a) Bifurcation diagram of single well PDM-Duffing oscillator with AM force for (a) $\Omega = 15$ and (b) Ω =30. Other parameter values of the system are fixed as $\omega_0^2 = 1, \beta = 1, d = 0.2, f = 0.05, \omega = 1.5, m_0 = 0.5, \lambda = 0$ and $f = 0.05$.

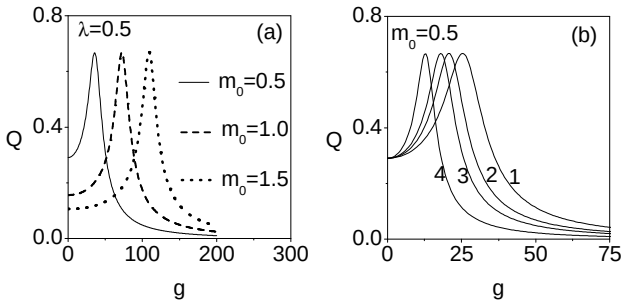

FIG. 4: (a)Numerical results for the variation of the response amplitude Q with g for (a) three values of mass amplitude m_0 and $\lambda = 0.5$ and (b) four values of λ and $m_0 = 0.5$. The values of λ for the curves $1-4$ are 1.0,1.5, 2.0 and 4.0 respectively. Other parameter values of the system are fixed as $\omega_0^2 = 1, \beta = 1, d = 0.2, f = 0.05, \omega = 1.5$ and $\Omega = 30.0$.

First we analyze the effect of the mass amplitude m_0 with $\lambda = 0.5$ on the observed resonance. Figure 4(a) shows the variation of Q with the control parameter g for three fixed values of $m_0(= 0.5, 1.0, 1.5)$ with $\lambda = 0.5$. When g is varied from the small value, single resonance occurs with same Q_{max} and the impact of g on Q is a shift in the peak position in the direction of increasing m_0. Then we compare the Fig.4(a) with Fig.2(d) which is plotted for the PDM parameters $m_0 = 0.5$ and $\lambda = 0$. In Fig.2(d), without the mass spatial nonlinearity ($\lambda = 0$), we obtain three resonances for $m_0 = 0.5$. When activating the mass spatial linearity λ, only one resonance is observed for all the values of m_0 which is clearly shown in Fig.4(a). The variation of the response amplitude Q with g for four values of $\lambda(= 1.0, 1.5, 2.0, 4.0)$ and $m_0 = 0.5$ is presented in Fig.4(b). Resonances with single peak

can be seen for all the values of λ with same Q_{max}. The position of the peak and width of the resonances decrease as λ increases which is clearly evident in Fig.4(b). In the absence of mass spatial nonlinearity ($\lambda = 0$), resonances observed in large interval of g (Fig.2) but when λ presents,we obtain resonances in a small interval of g. The dependence of the response amplitude Q on the frequencies Ω and ω of the AM force is shown in Fig.5. The variation of Q with g for three four values of $\omega(= 1.0, 2.0, 3.0, 5.0)$ with $\Omega = 30.0$ is shown in Fig.5(a). For $\omega = 1.0$, as g increases, Q decreases and resonance is not observed. For $\omega = 2.0, 3.0, 5.0$, resonance is found at $g = 55.24, 99.65$ and 175.73 respectively. In Fig.5(a), Q_{max} decreases as ω increases and at the time the position of the peak is shifted towards the high-frequency amplitude g. Figure 5(b) shows when g varies from 0 to 200, $m_0 = 0.5, \lambda = 0.5$ with $\omega = 1.5$ and the influence of the parameter Ω is shown on VR. From the Fig.5(b), we note that single resonance is observed for all values of Ω with almost same Q_{max}. Also there is a shift in the peak position in the direction of increasing g and width of the resonance increases as Ω increases.

Then, we analyze the effect of m_0 on the dynamics of the system with constant mass (ie., $\lambda = 0$) by looking the hysteresis and jump phenomenon. The values of the other parameters are $\omega_0^2 = 1, \beta = 1, d = 0.2, f = 0.05, m_0 = 0.5, \lambda = 0, \omega = 1.5$ and $\Omega = 30.0$. Fig.6(a) presents Q is obtained by varying g in the forward and reverse directions. Continuous curve obtained by varying the control parameter g in the forward direction and the dashed curve by varying the control parameter g in the reverse direction. We can clearly observe

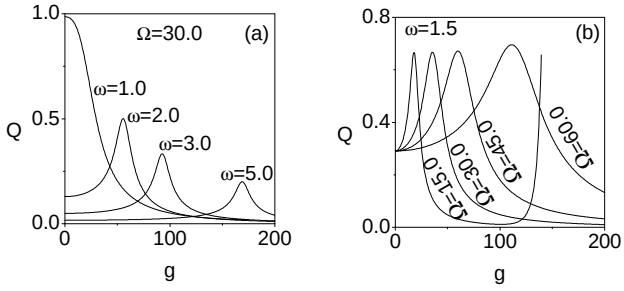

FIG. 5: (a) Numerical results for the variation of the response amplitude Q of the PDM-Duffing oscillator driven by an AM force with g for (a) four values of ω with $\Omega = 30$ and (b) for four values of Ω with $\omega = 1.5$. Other parameter values of the system are fixed as $\omega_0^2 = 1, \beta = 1, d = 0.2, m_0 = 0.5, \lambda = 0.5$ and $f = 0.05$.

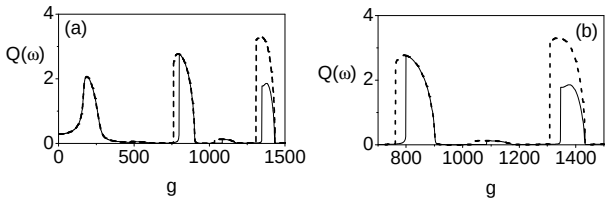

FIG. 6: (a) Response amplitude curve obtained by varying the control parameter g from 0 to 1500(continuous curve) and from 1500 to 0 (dashed curve) for the single-well PDM-Duffing oscillator system driven by an AM force. (b) Magnification of the $Q(\omega)$ curve in the interval $g \in [700, 1500]$ indicating hysteresis and jumps in Q. Other parameter values of the system are fixed as $\omega_0^2 = 1, \beta = 1, d = 0.2, m_0 = 0.5, \lambda = 0.0, \omega = 1.5, \Omega = 30.0$ and $f = 0.05$.

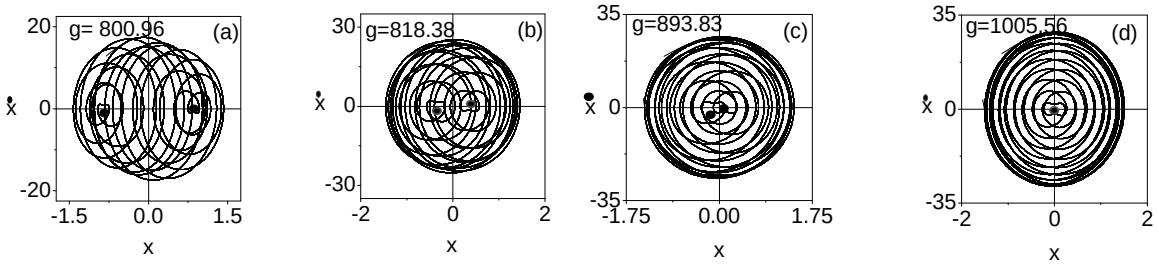

FIG. 7: Phase portrait of the system (Eq.8) for four values of g. The system is a single-well PDM-Duffing oscillator driven by an AM force. The parameter values of the system are as in Fig.6.

hysteresis and a jump phenomenon. Figure 6(b) shows the magnification of the Q curve in the interval $g \in [700, 1500]$. Q is found to follow different paths when g is varied in the forward and reverse directions. For the single well PDM-Duffing oscillator system, this phenomenon occurs at higher g values. To understand the dynamics of a single-well system with AM force, we consider the change in the phase diagram of the system. Figure 7 shows the portraits for four values of g in the interval $g \in [754.73, 1200]$. For $g = 800.96$, the orbit in the $x - \dot{x}$ plane consists of three parts. There is a part of the orbit enclosing both solid circles. In addition, we can clearly notice two other parts of the orbit-one enclosing left solid circle only and another right solid circle only. This is similar to an orbit moving around two equilibrium states. The distance between these two points decreases (and Q also decreases) with an increase in the value of g from 800.96. This is clearly evident from Figs.7(a)-((c).

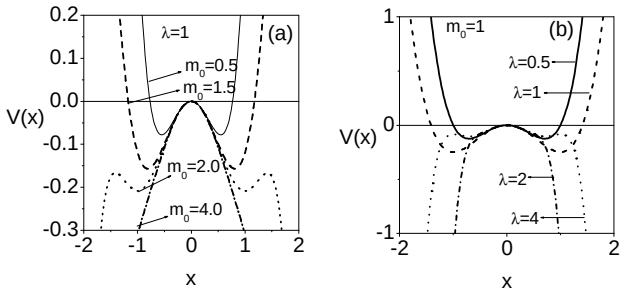

FIG. 8: (a) The system potential (Eq.9) for $d = 0.2, \beta = 1, \omega_0^2 = -1, \lambda = 1$ and $m_0 = 0.5, 1.5, 2.0, 4.0$ (b) The system potential (Eq.9) for $d = 0.2, \beta = 1, \omega_0^2 = -1, m_0 = 1$ and $\lambda = 0.5, 1, 2, 4$.

As shown in Fig.7(d) at $g = 1005.56$, the two points merged together at the origin and the orbit move around it like an orbit in a single-well potential. Q becomes a local minimum at this value of g.

4. VR in the Double-Well PDM-Duffing Oscillator

In the preceding section, we showed that the VR phenomenon can occur in the single-well system driven by an AM force. Now we proceed to verify the existence of VR phenomenon in double-well system driven by an AM force. We fix the mass parameter regimes within which the system potential is symmetrical double-well potential form so that $0 < m_0 < 1.5$ and $0 < \lambda < 1$ with $d = 0.2, \beta = 1$ and $\omega_0^2 = -1$. The system potential in Fig.8(a) and 8(b) for different values of the parameters : the mass amplitude $m_0 (= 0.5, 1.5, 2.0, 4.0)$ and the strength of the spatial nonlinearity $\lambda (= 0.5, 1, 2, 4)$ respectively is computed from the Eq.(9). First we examine the existence of VR phenomenon in the double-well system with constant mass (ie., $\lambda = 0$). The possibility of occurrence of VR through variation of the mass amplitude m_0 with the high-frequency amplitude g is confirmed by the results presented in Fig.9 for two values of frequency Ω of the high-frequency component of the AM force. Fig.9(a) presents the numerically computed response amplitude Q versus g for $\Omega = 15.0$. When $g < 125.25$ single resonance is obtained and $Q(\omega)$ does not decrease continuously beyond the first resonance peak. $Q(\omega)$ is maximum at more than one value of g and dense resonance peaks are observed in the region $402.15 < g < 500$. For $\Omega = 30$, $Q(\omega)$ decays to zero as g increases beyond g_{VR} (at which resonance occurs) which is clearly shown in Fig.9(b). Here only one resonance peak is possible. Hysteresis and a jump phenomenon are

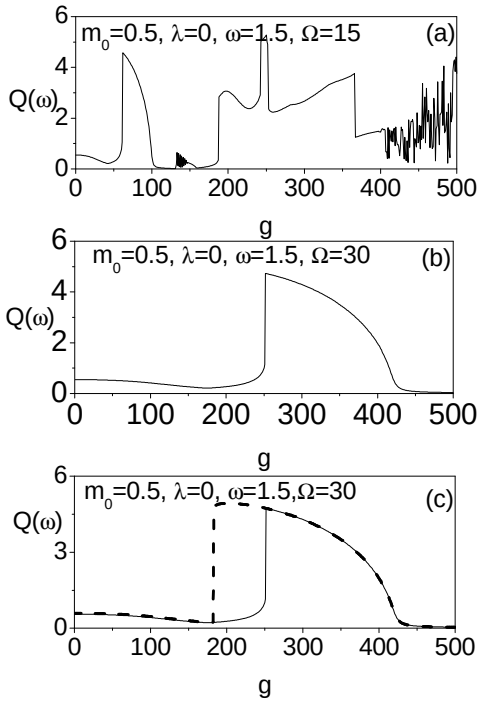

FIG. 9: Response amplitude Q curves for (a) $\Omega = 15$ (b) $\Omega = 30$ and (c) $Q(\omega)$ obtained by varying the control parameter g from 0 to 500 (continuous curve) and from 500 to 0 (dashed curve) for the PDM-Duffing oscillator with AM force. Other parameter values are $\omega_0^2 = -1, \beta = 1, d = 0.2, m_0 = 0.5, \lambda = 0.0, \omega = 1.5$ and $f = 0.05$.

also found in response amplitude curves when g is varies in forward and reverse directions. In Fig.9(c), Q is found to follow different paths as indicated by dashed lines where g is varied in the forward and reverse directions. Next we analyze the bifurcation structures of the system (Eq.8) for the two values of $\Omega(= 15, 30)$ and the corresponding bifurcation patterns is presented in Fig.10. The other parameter values of the system are as in Fig.9. In Fig.10(a), for increasing values of g, the periodic orbits dominates the dynamics in the high-frequency regime $0 < g < 398.55$ from which the value of g was chosen. For larger values of g, small periodic windows are sandwiched by chaotic regimes . The bifurcation pattern for $\Omega = 30$ is shown in Fig.10(b). For this case, only periodic states appear in the system which is clearly shown in Fig.10(b). For clarity an example of periodic and chaotic attractor from Fig.10(a) is shown in Figs.10(c) and 10(d).

So far we have investigated the occurrence of VR in the double-well PDM-Duffing oscillator system with constant mass ($\lambda = 0$). Further in order to know the contributions of the

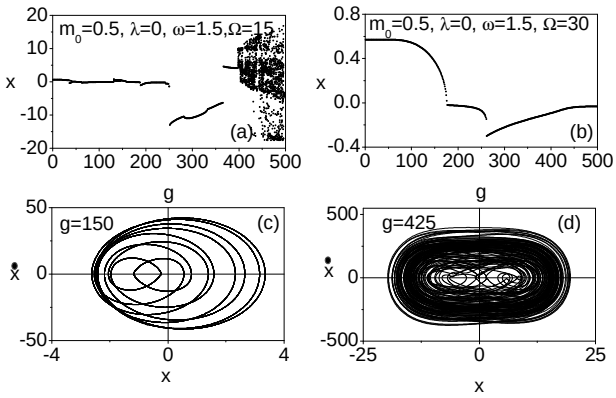

FIG. 10: Bifurcation diagrams of the double-well PDM-Duffing oscillator driven by an AM force for (a) $\Omega = 15$ and (b) $\Omega = 30$. Phase portraits of the system (c) periodic attractor and (d) chaotic attractor. The parameter values of the system are as in Fig.9.

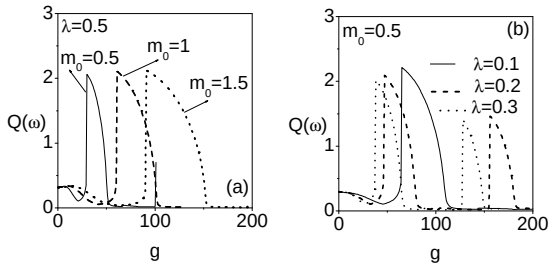

FIG. 11: The variation of the response amplitude Q with g for three values of (a) mass amplitude m_0 and $\lambda = 0.5$ and (b) mass spatial nonlinearity λ and $m_0 = 0.5$. Other parameter values of the system are fixed as $\omega_0^2 = -1, \beta = 1, d = 0.2, f = 0.05, \omega = 1.5$ and $\Omega = 30.0$.

mass spatial nonlinearity parameter λ to VR, we also consider the effect of λ on the observed resonances. First we showed that the resonances for $\lambda = 0.5$. This is presented in 11(a) for varying g and three values of $m_0 (= 0.5, 1, 1.5)$ respectively with $\omega = 1.5, \Omega = 30$. Q_{max} is almost the same in all the curves. But g_{max} and the width of the resonance curve increases with m_0. In Fig.11(b), $Q(\omega)$ is plotted for different values of λ and with $\omega = 1.5, \Omega = 30$. With increasing λ, double peaked resonances occur for $\lambda = 0.1$ and 0.2 and single peaked resonance occurs for $\lambda = 0.3$. Q_{max} is different for single and double peaked resonances and g_{max} (at which Q is maximum) and the width of the resonance curve decreases with λ increases, which is clearly shown in Fig.11(b).

Finally we study the dependence of Q on the frequencies ω and Ω of the driving forces.In

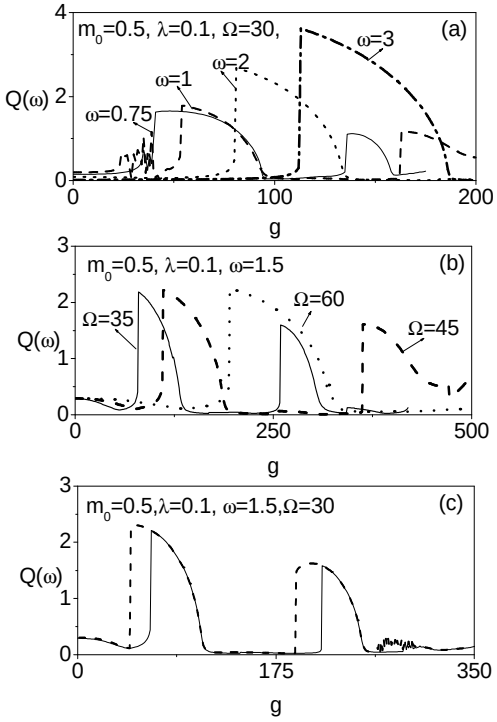

FIG. 12: Variation of the response amplitude Q of the PDM-Duffing oscillator driven by an AM force with g for (a) four values of ω with $\Omega = 30$ and (b) three values of Ω with $\omega = 1.5$. (c) $Q(\omega)$ obtained by varying the control parameter g from 0 to 350 (continuous curve) and from 350 to 0 (dashed curve) for the double-well PDM-Duffing oscillator with AM force. Other parameter values of the system are fixed as $\omega_0^2 = -1, \beta = 1, d = 0.2, m_0 = 0.5, \lambda = 0.1$ and $f = 0.05$.

Fig.12(a) $Q(g)$ is plotted for different values ω, namely, $\omega = 0.75, 1, 2, 3$ with $\Omega = 30, m_0 = 0.5, \lambda = 0.1$. With increasing ω, Q_{max} also increases. Fig.12(a) has double-peaked resonances for $\omega = 0.75$ and $\omega = 1$ while single-peaked resonance for $\omega = 2$ and $\omega = 3$. Width of the resonance curve and g_{max} values increase with increasing ω values. In 12(b) the resonance curve is plotted for different values of Ω for $\omega = 1.5$ with $m_0 = 0.5$ and $\lambda = 0.1$. Here we again observe that single and double resonances occur for different values of Ω. Q_{max} of the first and second resonances are almost the same in all the cases. But g_{max} and the width of the resonance curve increases with Ω. The hysteresis and a jump phenomenon in the double-well form of the potential of the system is confirmed by Fig.12(c) for $m_0 = 0.5, \lambda = 0.1, \omega = 1.5$ and $\Omega = 30$. For certain cases of the parametric choices considered in our study chaotic motion is found for sufficiently large values of the control parameter g, particularly, far after resonance. An example is presented in Fig.13(a) for $m_0 = 0.5, \lambda = 0.1, \omega = 1.5$ and $\Omega = 30$.

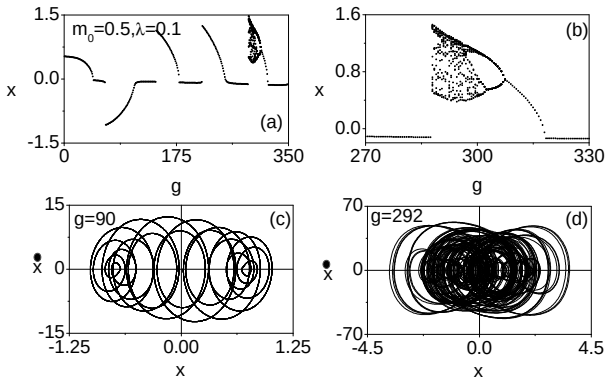

FIG. 13: Bifurcation diagrams of the double-well PDM-Duffing oscillator driven by an AM force for (a) $m_0 = 0.5, \lambda = 0.1, \omega = 1.5$ and $\Omega = 30$. (b) Magnification of a part of bifurcation diagram in Fig.13(a). Phase portraits of the system (c) periodic attractor and (d) chaotic attractor. The parameter values of the system are as in Fig.12.

For $0 < g < 330.12$, a period-T solution is found. When g is varied further reverse period-doubling phenomena leading to chaotic motion, intermittency and periodic windows occur and are clearly shown in Fig.13(b) which is a magnification of a small part of the bifurcation diagram Fig.13(a). For clarity, an example of periodic and chaotic orbits from Fig.13(b) is shown in Figs.13(c) and 13(d).

5. Conclusion

Generally in the VR studies a nonlinear system driven by a weak periodic force is further subjected to a high-frequency force with $\Omega \gg \omega$ while less attention is paid to different types of forces such as amplitude, frequency and pulse modulated forces. Also most of the previous VR investigations in a nonlinear system with constant mass and only few studies were reported in the system with position dependent mass. In the present work, we have analyzed the occurrence of vibrational resonance in the position-dependent mass (PDM)-Duffing oscillator system with single-well and double-well potentials driven by the amplitude modulated (AM) force. In the PDM-Duffing system, the mass is defined as a regular function comprising of mass amplitude m_0 and the strength of spatial nonlinearity λ. We investigated the existence of VR induced by the PDM parameters: m_0, λ and signal parameters: g, ω, Ω. From our numerical results, we found that the PDM parameters have significant effect on VR. Particularly, multiple resonance peaks and non-decaying behaviour of $Q(\omega)$ even for large values of the control parameter g are realized. Also period-doubling, reverse period-doubling

bifurcation, hysteresis and a jump phenomenon, intermittency dynamics and chaotic motion are realized in the PDM-Duffing system driven by an AM force. The use of the PDM and signal parameters have shown that the various complex phenomena obtained can be controlled and suppressed. Our investigations in this paper has potential applications in signal detection, transmission and amplification. Analysis of VR in PDM-Duffing oscillator system driven by frequency modulated (FM) force will be studied in future.

REFERENCES

[1] P.S. Landa and P.V.E. McClintock, *Vibrational Resonance*, J. Phys. A, **33** (2000) 1433-8

[2] M. Gitterman, *Bistable oscillator driven by two periodic fields*, J. Phys.A, **34** (2001) 1355-7.

[3] S. Jeyakumari, V. Chinnathambi, S. Rajasekar and M.A.F. Sanjuan, *Single and Multiple Vibrational resonance in a quintic oscillator with monostable potentials*, Phys. Rev.E,**80** (2009) 046608.

[4] S. Jeyakumari, V. Chinnathambi, S. Rajasekar and M.A.F. Sanjuan, *Analysis of vibrational resonance in a quintic oscillator*, Chaos, **19** (2009) 043128-8.

[5] S. Rajasekar, K. Abirami and M.A.F. Sanjuan, *Novel vibrational resonance in multistable systems*, Chaos **21(3)** (2011) 033106.

[6] E. Ullner, A. Zaikin, J. Garcia-Ojalvo, R. Bascones and J. Kurths, *Vibrational resonance and vibrational propagation in excitable systems*, Phys. Lett. A, **312** (2003) 348-354.

[7] H. Yu, J. Wang, C. Liu, B. Deng and X. Wei, *Vibrational resonance in excitable neuronal systems*, Chaos **21(4)**, (2011) 043101.

[8] B. Deng, J. Wang, X. Wei, K.M. Tsang and W.L. Chan, *Vibrational resonance in neuron populations*, Chaos, **20** 2010 013117

[9] U.E. Vincent, T.O. Roy-Layinde, O.O. Popoola, P.O. Adesina and P.V.E. McClintock, *Vibrational resonance in an oscillator with an asymmetrical deformable potential*, Phys. Rev. E **98(6)** (2018) 062203.

[10] T.O. Roy-Layinde, J.A. Laoye, O.O. Popoola and U.E. Vincent, *Analysis of vibrational resonance in bi-harmonically driven plasma*, Chaos **26(9)** (2016) 093117.

[11] J.H. Yang and X.B. Liu, *Controlling vibrational resonance in a delayed multistable system driven by an amplitude-modulated signal*, Phys. Scr. **82(2)** (2010) 025006.

[12] A. Daza, A. Wagemakers, S. Rajasekar and M.A.F. Sanjuan, *Vibrational resonance in a time-delayed genetic toggle switch*, Commun. Nonlin. Sci. Numer. Simul. **18(2)** (2013) 411-416.

[13] C. Wang and K. Yang, *Vibrational Resonance in Bistable Gene Transcriptional Regulatory System*, Chin. J. Phys. **50(4)** (2012) 607-617.

[14] V.N. Chizhevsky, E. Smeu, G. Giacomelli, *Experimental evidence of vibrational resonance in an optical system*, Phys. Rev. Lett. **91(22)** (2003) 220602.

[15] V.N. Chizhevsky, *Experimental evidence of vibrational resonance in a multistable system*, Phys. Rev. E **89(6)** (2014) 062914.

[16] R. Jothimurugan, K. Thamilmaran, S. Rajasekar and M.A.F. Sanjuan, *Experimental evidence for vibrational resonance and enhanced signal transmission in Chuas circuit*, Int. J. Bifur. & Chaos **23(11)** (2013) 1350189.

[17] A. Abusoua and M.F. Daqaq, *Experimental evidence of vibrational resonance in a mechanical bistable twin-well oscillator*, J. Comput. Nonlinear Dynam. **13(6)** (2018) 061002.

[18] Y. Ren and F. Duan, *Theoretical and experimental implementation of vibrational resonance in an array of hard limiters*, Physica A **456** (2016) 319-326.

[19] K.B. Wolf, *Geometric optics on phase space, Texts and Monographs in Physics*, Springer-Verlag, Berlin, 2004.

[20] A. Sommerfeld, *Lectures on theoretical physics*, Vol. I, Academic Press, New York, 1994.

[21] J. Flores, G. Solovey and S. Gil, *Variable mass oscillator*, Amer. J. Phys. 71 (2003) 721; https://doi.org/10.1119/1.1571838.

[22] J. Awrejcewicz, *Dynamics of systems of variable mass. In Classical Mechanics*, pp. 341 357. Springer, 2012.

[23] N. Aquino, G. Campoy, H. Yee-Madeira, *The inversion potential for NH3 using a DFT approach*, Chem. Phys. Lett. 296, (1998) 111116. (doi:10.1016/S0009-2614(98)01017-3)

[24] M.R. Bate, *Predicting the properties of binary stellar systems: the evolution of accreting protobinary systems*, Mon. Not. R. Astron. Soc. 314, (2000) 3353. (doi:10.1046/j.1365-8711.2000.03333.x)

[25] B.G. da Costa, I. Gomez, *Information-theoretic measures for a position-dependent mass system in an infinite potential well*, Physica A 541 (2020) 123698. (doi:10.1016/j.physa.2019. 123698).

[26] P.M. Mathews and M. Lakshmanan, *On a unique nonlinear oscillator*, Quart. Appl. Math. 32 (1974) 215; https://doi.org/10.1090/qam/430422

[27] S. Cruz y Cruz and O. Rosas-Ortiz, *Dynamical Equations, Invariants and Spectrum Generating Algebras of Mechanical Systems with Position-Dependent Mass*, SIGMA 9 (2013) 004; https://doi.org/10.3842/SIGMA.2013.004

[28] Oscar Rosas-Ortiz, *Position-dependent mass systems: Classical and quantum pictures*, arXiv:2002.02297v1 [physics.class-ph] 24th Jan 2020.

[29] B. Bhuvaneshwari, K. Amutha, V. Chinnathambi, S. Rajasekar, *Enhanced Vibrational Resonance by an Amplitude Modulated Signal in a Nonlinear Dissipative Two-Fluid Plasma Model*, Contributions to Plasma Physics, e202100099, (2021) pp. 1-10, https://doi.org/10.1002/ctpp.202100099,

[30] B. Bhuvaneshwari, S. Valli priyatharsini, V. Chinnathambi and S. Rajasekar, *Effect of modulated signals on VR in a harmonically trapped potential system*, Journal of Scientific Research , 13(3), (2021) 797-807

[31] B. Bhuvaneshwari, S. Valli Priyatharsini, V. Chinnathambi and S. Rajasekar, *Dynamics of Nonlinearly Damped Duffing-vander Pol Oscillator Driven by Frequency Modulated Signal*, Nonlinear Dynamics and Systems Theory, 21(5) (2021) 1-10

[32] S. Guruparan, V. Ravichandran , V. Chinnathambi and S. Rajasekar, *Coexistence of Multiple attractors , Hysteresis and Vibrational resonancein the classical Morse oscillator driven by an amplitude modulate signal*, Ukraine Journal of Physics, **62(1)** (2017) 51-59.

[33] O. Mustafa, *Comment on nonlinear dynamics of a position-dependent massdriven Duffing-type oscillator*, J. Phys. A: Math. Theor. 46, 368001. (2013) (doi:10.1088/1751-8113/ 46/36/368001).

[34] Cruz SCY, O. Rosas-Ortiz, *Dynamical equations, invariants and spectrum generating algebras of mechanical systems with position-dependent mass*, Symmetry Integr. Geom. **9** (2013) 421.

[35] T.O. Roy-Layinde, U.E. Vincent, S.A. Abolade, O.O. Popoola, J.A. Laoye and P.V.E. McClintock, *Vibrational resonances in driven oscillators with position-dependent mass*, Phil. Trans. R. Soc. A 379: 20200227. (2020) https://doi.org/10.1098/rsta.2020.0227.)